Frequency variation under constant power conditions in hydrogen radio frequency discharges

E. Amanatides and D. Mataras[a)]
Plasma Technology Laboratory, Department of Chemical Engineering University of Patras, P.O. Box 1407, 26500 Patras, Greece

(Received 20 June 2000; accepted for publication 8 November 2000)

The effect of driving frequency (13.56–50 MHz) on the electrical characteristics and the optical properties of hydrogen discharges has been studied, under constant power conditions. The determination of the discharge power and impedance was based on current and voltage wave form measurements, while at the same time spatially resolved H_α emission profiles were recorded. As frequency is increased, the rf voltage required for maintaining a constant power level is reduced, while the discharge current increases and the impedance decreases. Concurrently the overall H_α emission intensity decreases and its spatial distribution becomes more uniform. Further analysis of these measurements through a theoretical model reveals that frequency influences the motion of charged species as well as the electron energy and the electric field, resulting in a modification of their spatial distribution. Moreover, the loss rate of charged species is reduced, leading to an increase of the plasma density and to a decrease of the electric field. Under these conditions, the total power spend for electron acceleration increases with frequency, but combined to the higher electron density, leads to a drop of the average energy gained per electron, a drop of the mean electron energy, and an enhancement of the low-energy electron-molecule collision processes against high energy ones. © *2001 American Institute of Physics.* [DOI: 10.1063/1.1337597]

I. INTRODUCTION

Capacitively coupled rf glow discharges, operating at the industrial frequency of 13.56 MHz, are widely used as sources of reactive species for plasma deposition, etching, or surface treatment. Alternatively, the use of very high frequency has been proposed by some authors as leading to higher deposition and etching rates.[1,2] As a result, a growing number of experimental and theoretical studies concerning the issue have appeared in literature during the last few years. From the theoretical point of view: A particle in cell/Monte Carlo (PIC/MC) simulation[3] of helium glow discharges has been used to reveal changes in the discharge structure at frequencies between 30 and 120 MHz. The results show that the plasma density and the rf current scale as the square of the applied frequency while the plasma potential is not affected and the sheath length varies almost inversely with frequency for a given rf voltage. A verification of these frequency-scaling laws combined with a more precise analysis of the uniformity and directionality of the ion flux towards the surfaces has been performed using a two-dimensional (2D) PIC/MC simulation at conditions of constant applied voltage.[4] Moreover, self-consistent fluid equations have been used by Colgan *et al.*[5] to study structural features of argon discharges at frequencies ranging from 13.56 to 54.4 MHz. The effect of frequency on plasma density, sheath lengths, power consumption, and plasma potential at conditions of fixed voltage and fixed rf current have been reported and have been compared to the earlier-mentioned PIC/MC simulations.

Concerning experimental studies, the most important difficulty in performing a true only frequency dependent experiment, is to ensure the proper discharge and external circuit conditions. Moisan *et al.*[6] in a review article concerning surface-wave discharges (SWDs) have proposed that in order to compare different frequency plasmas, one has to maintain a constant electron density. As this condition is difficult to be achieved experimentally, constant power dissipation that in the case of SWDs corresponds to constant total electron power has been alternatively proposed in an attempt to isolate frequency effects from the influence of other discharge parameters as much as possible.

Following this method in capacitively coupled discharges, the effects of frequency on silane plasmas and more precisely on the deposition rate of *a*-Si:H, as well as on the dissociation and dissociative excitation rates of silane, have been reported.[7,8] These studies have shown that the deposition rate and the gas phase processes are both enhanced by the increase of frequency in the range from 13.56 to 70 MHz. Silane discharges have also been studied by another group for frequencies varying between 40 and 250 MHz again under constant power conditions.[9] Their results show a slight increase of the silane dissociation and an almost constant dissociative excitation rate, while the observed increase of the deposition rate is attributed to an enhanced surface reactivity of the film precursors.[9] In addition, Kitajima *et al.*[10] have reported 2D time-resolved profiles of Ar excitation rate and reported a more efficient production of excited species and a higher plasma density at 100 MHz compared to 13.56 MHz.

Although, through these studies, a significant progress in the understanding of frequency effects on discharge proper-

a)Electronic mail: dim@chemeng.upatras.gr

ties has been achieved, the results concerning the enhancement of high-energy processes with frequency appear to be controversial. The discrepancies found in literature are believed to be mainly due to the following reasons. First, theoretical studies have been mainly focused on the simulation of noble gas discharges in constant voltage conditions, thus no information is available on the effect of frequency on plasma structure and density under constant power dissipation. Second, the proper discharge conditions that lead to constant power dissipation depend strongly on discharge parameters like the gas mixture, the pressure or the interelectrode distance; these parameters have to be taken into account when comparing results from different groups. Third, in the case of capacitively coupled discharges in contrast to SWDs, the constant power dissipation is not consequently followed by constant electron power and the fraction of the power consumed for ion acceleration in the sheaths has to be considered. Finally, an accurate determination of the real power consumed in the discharge is required. In all the experimental studies mentioned earlier, the power actually consumed in the discharge has been determined using the subtractive method. At 13.56 MHz, this rather simple method gives comparable results with other more precise methods.[11] However, in the case of variable frequency operation, a very careful design of the matching network is required in order to minimize losses in the external network, and to avoid instabilities and matcher nonlinearity due to temperature changes, over the entire range of frequencies studied. In both cases[9,10] the accuracy of the method is questionable because readjustment of the forward power and retuning of the matching network during the measurements have been reported.

The present work attempts to clarify the effect of frequency on electron impact processes under constant power conditions, assured by a much more accurate method involving current and voltage measurements at the powered electrode.[12] For this purpose, a study of pure hydrogen discharges at the frequency range between 13.56 to 50 MHz has been performed. Hydrogen has been preferred instead of a noble gas, as in most plasma etching and deposition processes molecular gases are used. In these cases, the rotational and vibrational excitation of molecules, from impact with low-energy electrons, will strongly influence power dissipation, electron energy, momentum, and energy transfer collision frequency. As these parameters with respect to the change of the rf period, are very important when comparing discharges at different excitation frequencies, hydrogen is expected to simulate better processes that involve other molecular gases. In addition, hydrogen is very often used as a buffer gas in the deposition of microcrystalline silicon and diamond like carbon.

The values of voltage, current, and impedance, that are required for constant power dissipation as frequency is varied, are firstly discussed and then used in an theoretical model of rf discharges, together with spatially resolved optical emission spectroscopy measurements of the α Balmer line of atomic hydrogen. The results are thoroughly discussed against other experimental findings concerning the issue,[7–10,13] while a comparison with theoretical predictions based on the solution of the time-dependent Boltzmann equation for hydrogen discharges[14,15] is also performed.

II. EXPERIMENT

A capacitively coupled UHV parallel plate system, having a base vacuum of 10^{-9} Torr has been used in this work. The 120 mm in diameter rf electrode is fixed to the chamber while the 90 mm in diameter grounded electrode can be moved to vary the interelectrode distance. For this series of experiments, the electrode distance is set at 17 mm. The rf electrode is powered by a Dressler WLPG 101D wideband (5–125 MHz) generator, through an L-type matching network. A fcc model F-35-1 current probe and a Lecroy PPE 100:1 attenuating voltage probe are attached to the power lead after the matching network. Voltage and current signals are recorded using a Lecroy 9400 digital oscilloscope and then transferred to a computer for Fourier analysis. The method for the measurement of the real power consumed in the discharge at 13.56 MHz has been presented in detail elsewhere.[12] In this method an electrical equivalent circuit accounting for the stray impedance of the cell is used in order to convert the current and voltage wave forms, measured outside the chamber to equivalent waveforms at the rf electrode. A shunt circuit is externally connected for increasing the accuracy of the method, while the electrical circuit is complemented to account for power losses in a stray resistance in both the shunt circuit and the cell itself. In the present case, fast Fourier transform and the counterbalance of cell and shunt resistance increase phase shift resolution accuracy.[11] However, at frequencies higher than 13.56 MHz, phase shift errors can be due to the probe bandwidths.[16] Thus, in order to check the applicability of the method at the range of frequencies studied here, a procedure analogous to that in Ref. 17 has been followed. The empty cell has been excited at different frequencies and the results were used to calculate the inductive L, capacitive C, and resistive R components of the cell. The experimental measurements and the fitting with the RLC model used for the calculation of voltage and current wave forms on the rf electrode are shown in Fig. 1. The excellent agreement between the experimental and the RLC model results, confirms the applicability of the method at least up to 50 MHz. These results are used to derive the following electrical characteristics of the reactor: inductance $L=40$ nH, capacitance $C=285$ pF, resistance $R=0.8\ \Omega$, and a resonance reactor frequency of 43 MHz.

In all cases, ultrahigh purity hydrogen (BOC, ultra large scale integration 99 9999%) is fed in the reactor at a flow rate of 20 sccm and a total pressure of 500 mTorr. Pressure and flow rate are independently adjusted by a downstream throttle valve controller and an upstream mass flow controller, respectively.

The experimental setup used for recording emission intensity profiles of excited radicals has been described in detail elsewhere.[18,19] The difference in the present case is that instead of moving the reactor for recording emission intensity from a specific discharge volume, the optical system, consisting of two slits and an optical fiber manifold, is moved.

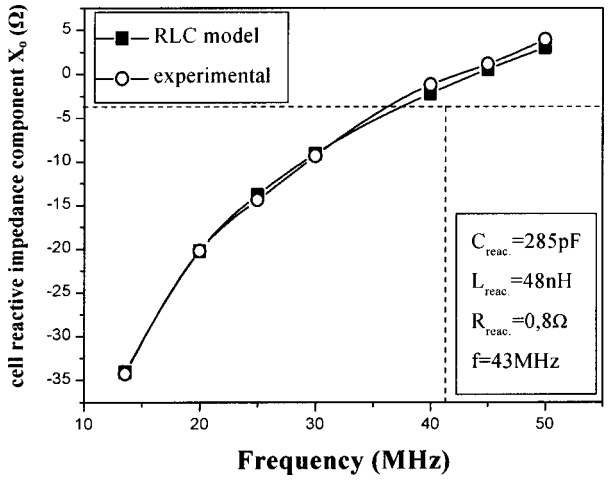

FIG. 1. The reactive component of the chamber impedance, as a function of the excitation frequency, resulting from experimental measurements and RLC equivalent circuit model.

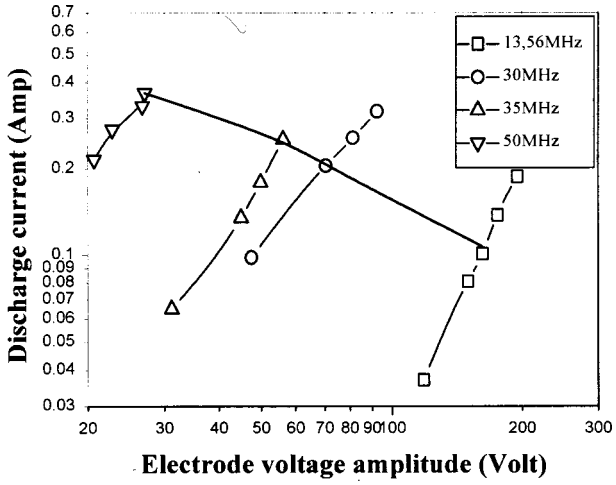

FIG. 3. Total discharge current as a function of the electrode voltage amplitude at the conditions of Fig. 2. The solid line represents constant power dissipation of 40 mW/cm^2.

III. RESULTS

Different sets of power and impedance measurements have been performed for 500 mTorr H_2 discharges, at excitation frequencies of 13.56, 30, 35, and 50 MHz. The variation of the discharge power density as a function of the electrode voltage amplitude is presented in Fig. 2. As frequency increases, a significant drop of the amplitude of the voltage required to operate the discharge at the same power level is observed (solid line, Fig. 2). A similar behavior has also been observed in all the studies that concern frequency variation under constant power conditions,[7,9,10] however, with a less pronounced drop. In the present case the electrode voltage amplitude, scales with frequency as $V_{el} \propto \omega^{-1/2}$, pointing out two important parameters that should be strongly affected by the change of the driving frequency. First, the power consumed for ion (P_i) and electron (P_e) acceleration, depend on the discharge voltage in a different manner and thus, changes on their relative contribution in the total discharge power are expected. Second, the significantly different values of voltage required for constant power dissipation reflect changes of the balance between ionization and charge loss rates. The charge loss rate is strictly related to the ion conduction current in the sheaths that, as it will be shown in Sec. IV A, decreases with frequency and this will probably affect the ionization rate.

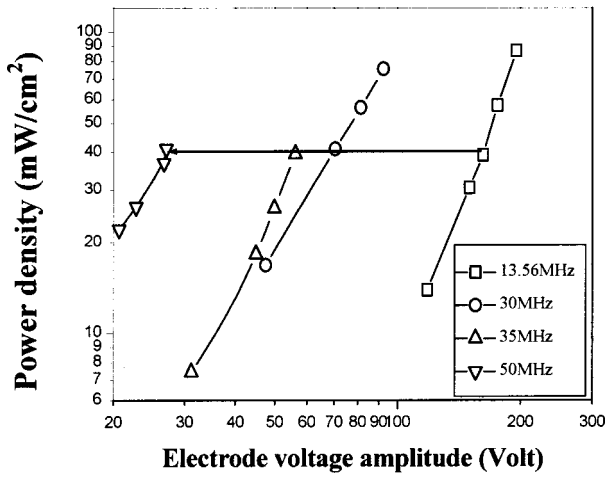

FIG. 2. Power consumed in the discharge as a function of the powered electrode voltage amplitude in 0.5 Torr hydrogen discharges at four different driving frequencies. The solid line represents constant power dissipation of 40 mW/cm^2.

Information concerning the power dissipation for ions and electrons acceleration can be extracted from the discharge current since the ratio between P_i and P_e at a fixed pressure and electrode distance,[20] scales as $P_i/P_e \propto (I/\omega^2)$. The total discharge current as a function of the electrode voltage amplitude is plotted in Fig. 3. For constant power dissipation, the discharge current is more than doubled, scaling as $I \propto \omega^{1.2}$ (solid line, Fig. 3) and thus the ratio P_i/P_e decreases with frequency, revealing that a larger fraction of power will be consumed for electron heating as frequency increases.

Except for the information concerning power dissipation, the current flow in the discharge can also be used for the estimation of the effect of frequency on the discharge electric field and the electron density. This can be done by taking into account the different manner of current conduction in the bulk and in the sheaths. The time-varying total current density J in the discharge can be expressed as the sum of the ion conduction J_i, the electron conduction J_e and the displacement current J_d:

$$J = J_i + J_e + J_d = e n_i u_+ + e n_e u_e + \omega \varepsilon_0 E, \tag{1}$$

where E is the rf Electric field, n_i, n_e the ion and the electron density respectively, u_+, u_e the ion and electron drift velocity, e the electron charge, and ε_0 the permittivity of vacuum.

The displacement current is expected to dominate in the sheaths[17] and thus in this case eq. (1) can be rewritten as

$$J \approx J_d = \omega \varepsilon_0 E. \tag{2}$$

Taking into account the relative increase of the discharge current and frequency, Eq. (2) indicates that for constant

TABLE I. The values of the sheath fields and lengths E, d, ion conduction current density J, and average charge density n_{av}, as calculated from the model of ion transport in the bulk and in the sheaths, at conditions of constant power dissipation.

Frequency (MHz)	E_{dp} (V/cm)	E_{dg} (V/cm)	E_{op} (V/cm)	E_{og} (V/cm)	J_{ip} (mA/cm^2)	J_{ig} (mA/cm^2)	d_{pd} (cm)	d_{gd} (cm)	n_{av} (10^8 cm^{-3})
13.56	174	76	25	16	0.024	0.014	0.85	0.42	2.95
30	135	72	21	12	0.018	0.012	0.61	0.37	3.98
35	141	74	19	11	0.017	0.011	0.55	0.32	5.12
50	142	78	17	9	0.014	0.010	0.48	0.27	6.72

power dissipation, the time averaged field in the rf electrode drops significantly from 13.56 to 30 MHz and remains almost constant from 30 to 50 MHz (see Table I, Sec. IV).

On the other hand, in the bulk plasma, the current flow is almost completely due to electrons, and thus Eq. (1) becomes in this case

$$J \approx J_e = e n_e u_e = e^2 n_e \frac{E_b}{m_e \sqrt{v_m^2 + \omega^2}}, \tag{3}$$

where n_e is the electron density, E_b the bulk field, v_m the momentum transfer collision frequency, and m_e the electron mass.

According to Eq. (3) the increase of the current density observed at higher frequencies (Fig. 3) at constant power dissipation, will be a combined result of changes in the electron density, the bulk electric field, and the momentum transfer collision frequency. In turn, the bulk field and the collision frequency depend on changes in the electron energy.

The existing literature includes controversial results concerning the influence of frequency on electron energy and density. Thus, according to Heintze *et al.*,[9] electron temperature and density remain almost constant in the range between 40 and 250 MHz. On the other hand, Yan and Goedheer[21] predict an increase of electron density and a decrease of electron temperature as frequency varies from 13.56 to 65 MHz. Moreover, in conditions of constant bulk field that have been proposed by Beneking[17] as describing very well discharges operating at different frequencies, a solution of the Boltzmann equation predicts an increase of the electron energy.[15] Thus, since existing data do not permit the extraction of unambiguous conclusions for the estimation of these parameters at the present experimental conditions, further analysis is needed.

The discharge impedance can reveal information concerning the electron-molecule collision frequency and the bulk field. The complex discharge impedance is given by[12]

$$Z = \frac{V_{el}}{I_{el}} e^{j\varphi_{el}} = R + jX, \tag{4}$$

where φ_{el} is the phase of the electrode voltage V_{el}, relative to the electrode current I_{el}.

The ohmic component of the impedance that can be attributed to the power dissipation in the discharge, is given by

$$R = \frac{V_{el}}{I_{el}} \cos\phi_{el}. \tag{5}$$

This can be further analyzed to:[22]

(a) The plasma resistance R_v corresponding to electron molecule collisions,
(b) an additional plasma resistance R_{st} corresponding to stochastic collisions of electrons with the oscillating plasma-sheath boundary, and
(c) a parallel or in series sheath resistance R_i accounting for ion acceleration in the sheaths.

The reactive part of the discharge impedance is given by

$$X = \frac{V_{el}}{I_{el}} \sin\phi_{el} \tag{6}$$

with X being the result of the competitive capacitive and inductive behavior of the sheath and bulk plasma, respectively. At 13.56 MHz electrons suffer many collisions per rf cycle, and thus the usual estimation is that they oscillate in phase with the bulk electric field (pure ohmic bulk), the out of phase motion of electrons being neglected. However, the out of phase oscillation of electrons increases with frequency. During this motion, electrons cannot impart any energy to the gas. The importance of this stochastic motion, and its weight in the reactive part of the impedance, will depend on the ratio of excitation frequency to the electron-molecule collision frequency ω/v_m.

In Fig. 4(a) the total resistive component R is plotted as a function of the discharge current. A decrease of the resis-

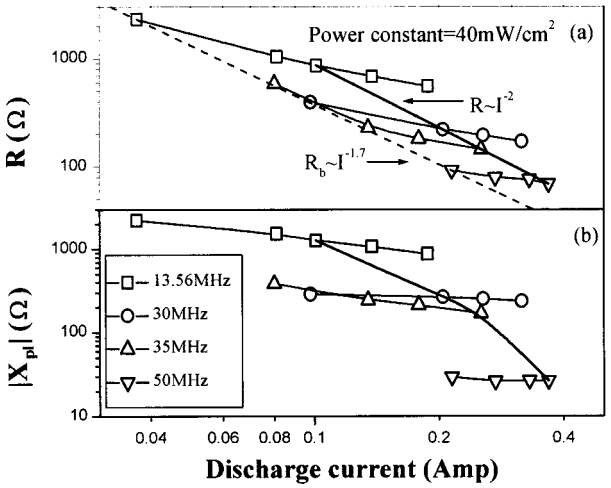

FIG. 4. Resistive (a) and reactive (b) part of the discharge impedance as a function of the total discharge current at four different excitation frequencies. Solid lines represent constant power consumption while the dashed line in (a) is an approximation of constant bulk field.

tive part of the discharge impedance is observed at higher frequencies. This decrease, according to the earlier analysis, can be a result of a decrease of the electron energy, which will strongly influence electron-molecule collision frequency, and/or an increase of the electron density. Moreover, it can also be a result of a decrease of the power consumed for ion acceleration in the sheaths, while stochastic collisions at this pressure (500 mTorr) can be neglected. The solid line in Fig. 4(a) is again the line of constant power, while the dashed line is approached by $R=f(I)$ curves at low currents. The observation that this curve describes a relation of the form

$$R=\text{const}\times I^{m}(m\approx -1) \tag{7}$$

has been used by Beneking[17] to calculate bulk field values suggesting that the field remains almost constant, independent of frequency. In the present case the approximation of a constant bulk field, is not accurate ($m\approx -1.7$) and thus the bulk field value cannot be calculated using this assumption. However, a relation of the form $R\propto I^{-1.7}$ [dashed line, Fig. 4(a)] indicates a drop of the bulk field with frequency. A reduction of the bulk field will be followed by a decrease of the electron drift velocity. Thus, the higher current flows that have been observed (Fig. 3), according to the analysis of current conduction in the bulk [Eq. (3)], impose the requirement of an increased electron density. This increase is verified by a more precise study of the charge transport in the bulk that will be presented in Sec. IV B.

The increase of plasma density with frequency will be followed by changes in the discharge structure, i.e., a decrease of the sheath lengths. This decrease will lead to an increase of the sheath capacitance and consequently to a reduction of the discharge reactance.[12] This is reflected in Fig. 4(b) where the absolute value of the discharge reactance X_{pl}, at conditions of constant power dissipation (solid line), shows a significant drop with frequency.

These changes in the discharge structure, together with information concerning the effect of frequency on the ionization rate, can also be extracted from emission measurements. Thus, Fig. 5 shows axial emission profiles of the electronically excited H_{α}, at different excitation frequencies, under conditions of constant power dissipation. This process in pure hydrogen discharges, results from one electron impact dissociative excitation of molecular hydrogen[23] and its energy threshold and cross section are very close to those of the one electron impact ionization process

$$\mathrm{H_2}+e\rightarrow \mathrm{H}^{*}(n=3\rightarrow 2)+\mathrm{H}(1s)\quad 16.6\ \text{eV}$$

$$\mathrm{H_2}+e\rightarrow \mathrm{H_2^{+}}+2e\quad 15.4\ \text{eV}.$$

This allows the use of emission profiles (Fig. 5) as an approximation of the time averaged ionization rate function in space.

It is obvious from Fig. 5 that the effective electron population for this specific process is reduced at higher frequencies. Under these conditions, the interaction of electrons with the high-field oscillating sheath is the main electron heating mechanism, producing electrons that have energy above the threshold of the specific process. Thus, the drop of the sheath field that has been predicted, using the displacement current

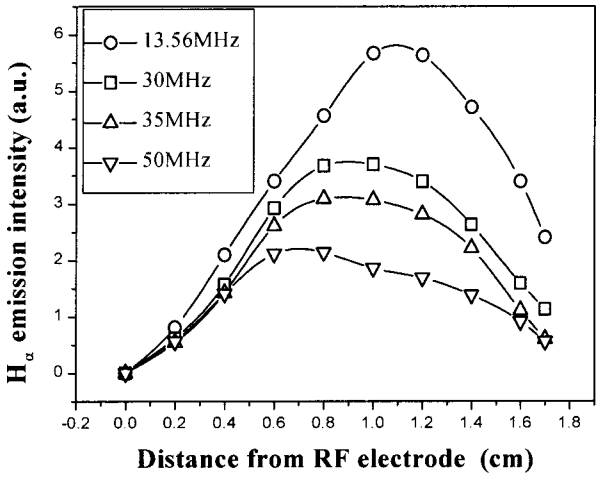

FIG. 5. Spatial distribution of H_{α} emission intensity in 500 mTorr hydrogen discharges at four different excitation frequencies and conditions of constant power dissipation.

[Eq. (2)] can be responsible for the drop of emission intensity with increasing frequency. Furthermore, at higher frequencies, the maximum excitation rate moves closer to the powered electrode, confirming the reduction of the sheath lengths estimated from impedance measurements.

To summarize the observations based on the experimental results presented so far, the sheath electric field and the sheath lengths decrease, while the fraction of power transferred to electrons increases with frequency, under constant power conditions. The emission measurements verify the decrease of sheath lengths and show that the population of electrons having energy above 16.6 eV decreases with frequency. Only suggestions have been made about the increase of electron density and the drop of electron energy, ionization, and charge loss rates with frequency. These need to be verified by the following theoretical analysis.

IV. ANALYSIS

The model used in this study has similarities to that presented by Lieberman,[24] in the sense that the discharge is distinguished in sheaths and bulk and uses an expression of the form of Child's law for the sheaths. It is one dimensional and the basic assumptions that have been used are:

(a) Ions respond only to the time-averaged electric field and the ion motion is collisional with a constant mean free path.

(b) The time-averaged values of the electric field and the electron density in the rf sheath have been calculated assuming that the sheath-plasma boundary oscillates as $d_s(t)=d_p(1+sin\,\omega t)$. Results for the sheath of the grounded electrode have been extracted by shifting the phase of solution of rf sheath by $\omega t=\pi$.

(c) An ambipolar transport in the bulk has been assumed and although the electron distribution function is not expected to be Maxwellian, a use of electron temperature has been made for an initial estimation of the ambipolar dc field and the determination of ambipolar diffusion coefficient.

The formulation of the model is not self-consistent in the sense that it requires the self-bias voltage, the discharge current, the ohmic part of the discharge impedance, and the spatial distribution of the ionization rate. The output parameters of the model are the spatial distribution of electrons and ions, the distribution of the electric field, the power dissipation to ions and electrons, and the mean electron energy.

A. Ion transport in the sheaths

The transport of ions in the sheath is usually described as a collisionless or collisional, space charge limited motion. The charge conservation condition and the assumption of no ionization or recombination in the sheath impose the requirement of a constant ion flux. In reality, ion density gradually decreases while ion drift velocity increases, from the plasma sheath boundary towards the rf electrode:[25]

$$J_i = e n_i(x) u_+(x), \tag{8}$$

where, $n_i(x)$ the ion density and $u_+(x)$ the ion drift velocity.

The ion mean free path λ_+ of hydrogen ions in 500 mTorr H_2 discharges is about 0.2 mm being much smaller than the sheath thickness in any case.[26] Thus, the mobility solution of the Child–Langmuir law[27,28] for a collisional sheath, can be used to calculate the ion flux. The values of the sheath electric fields are expected to be high enough in the conditions studied here, allowing thus to express the ion drift velocity in the sheath using the high-field mobility factor

$$u_+ = k\sqrt{\frac{E}{P_g}}, \tag{9}$$

where the value of $k(61\ \mathrm{m^{3/2}\,Torr^{1/2}/V^{1/2}\,s})$, obtained by interpolating mobility data.[29]

By combining Eq. (9) to Poisson's equation $[dE/dx = e n_i(x)/\varepsilon_0]$, the expression of ion current density [Eq. (8)] is transformed to a relation of the form of Child's law

$$J_i = \frac{2}{3} k \varepsilon_0 \left[\frac{\overline{E}^{3/2} - \overline{E}_0^{3/2}}{x}\right], \tag{10}$$

where $\overline{E}$ is the time averaged value of the sheath field at the position x, and $\overline{E}_0$ is the value of the electric field at the plasma-sheath boundary ($x=0$). The use of nonzero value of the field at the plasma-sheath edge is necessary to eliminate the singularity for the ion density in the collisional case,[30] while the value of $\overline{E}_0$ is determined by the relation $\overline{E}_0 = T_e/\lambda_D$ describing the plasma sheath transition.

According to Eq. (9) for constant ion flux, the distribution of the time-averaged field in the sheath can be written as

$$\overline{E}(x) = \sqrt[3]{\left((\overline{E}_d^{3/2} - \overline{E}_0^{3/2})\left(\frac{x}{d}\right) + \overline{E}_0^{3/2}\right)^2}, \tag{11}$$

where d is the mean sheath thickness and E_d the field value at the electrode.

The distribution of the electric field can then be combined to Poisson's equation to calculate the ion density distribution

$$N_i(x) = \frac{2\varepsilon_0(\overline{E}_d^{3/2} - \overline{E}_0^{3/2})}{3ed}\left[(\overline{E}_d^{3/2} - \overline{E}_0^{3/2})\left(\frac{x}{d}\right) + \overline{E}_0^{3/2}\right]^{-1/3} \tag{12}$$

and the voltage distribution in the sheath

$$\overline{V} = \frac{3d}{5(\overline{E}_d^{3/2} - \overline{E}_0^{3/2})}\left((\overline{E}_d^{3/2} - \overline{E}_0^{3/2})\left(\frac{x}{d}\right) + \overline{E}_0^{3/2}\right)^{5/3} - \frac{3d\overline{E}_0^{5/2}}{5(\overline{E}_d^{3/2} - \overline{E}_0^{3/2})}. \tag{13}$$

Furthermore, the electrons in the sheath are assumed to be in Boltzmann equilibrium and have a Maxwellian distribution. Therefore, the electron density distribution is of the form[31]

$$\overline{n_e}(x) = \overline{n_e}(0)\exp\left(\frac{\overline{V}(x) - \overline{V}(0)}{T_e}\right), \tag{14}$$

where $\overline{n_e}(0)$ and $\overline{V}(0)$ is the electron density and the voltage at plasma-sheath boundary.

The time-averaged values of the electric field and the sheath thickness, required for the solution of the set of Eqs. (9)–(13), are calculated as follows: The mean values of the powered and grounded sheath lengths are found assuming a pure capacitive nature of the two sheaths. The power and grounded sheath reactive impedances can be distinguished, and the sheath lengths can be then calculated using[32]

$$d_{\mathrm{pd}} = \frac{V_{\mathrm{pd}}\omega A\varepsilon_0}{I_d} \quad \text{and} \quad d_{\mathrm{gd}} = \frac{V_{gd}\omega A\varepsilon_0}{fI_d}, \tag{15}$$

where I_d is the total discharge current and f a factor related to the fraction of the total current conducted by the grounded electrode[33], with respect to the applied voltage for each frequency.

The values of the sheath fields E_d at $x=d$ are calculated using Eq. (3), with the assumption that almost all of the sheath current is a displacement current

$$E_{\mathrm{pd}} = \frac{I_d}{\omega\varepsilon_0 A} + E_{\mathrm{op}} \quad \text{and} \quad E_{\mathrm{gd}} = \frac{fI_d}{\omega\varepsilon_0 A} + E_{\mathrm{og}}. \tag{16}$$

For the values of the field at $x=0$ (sheath-bulk interface) the Godyak–Sternberg model[30] for the presheath is used and $\overline{E}_0$ is calculated by equalizing the velocity of ions injected from the plasma into the sheath with the velocity of ions in the sheath, in Eq. (9):

$$\sqrt{\frac{T_e q}{M_i}}\left(1 + \frac{\pi\lambda_D}{2\lambda_i}\right)^{-1/2} = k\sqrt{\frac{E_0}{P}} \Rightarrow \frac{T_e}{\lambda_D} = T_e\left(\frac{qP}{M_i k^2} - \frac{\pi}{2\lambda_i}\right). \tag{17}$$

The necessary electron temperature estimation results in this case from equation

$$V_{\mathrm{dc}} + V_p = \frac{T_e}{2}\ln\sqrt{\frac{M_i}{2.3m_e}} + T_e \ln\left\{I_0\left[\frac{(1-f)V_{el}}{T_e}\right]\right\}, \tag{18}$$

with V_p the plasma potential, and I_0 the zero-order modified Bessel function of the first kind.

B. Ion transport in the bulk

In order to relate the time-averaged values of the field and the charged particle densities in the sheaths to their values in the bulk, ambipolar diffusion dominated ion transport is considered [29]

$$-D_a \frac{\partial^2 N}{\partial x^2} = S(x), \tag{19}$$

where $S(x)$ is the time averaged ionization rate in space and D_a is the ambipolar diffusion coefficient. $S(x)$ is approximated using the emission profiles of the α Balmer line of atomic hydrogen (Fig. 5). Hydrogen being an electropositive gas, electron-ion recombination can be neglected, and due to the low ion densities, the same is true for ion–ion recombination.

The ambipolar diffusion coefficient D_a, is determined by the electron temperature and the ion mobility

$$D_a = \mu_+ \frac{kT_e}{e}. \tag{20}$$

Since, the values of the electric field in the bulk are expected to be rather weak, a low field mobility[34] of $\mu_+ P_g = 0.92$ ($m^2\ V^{-1}\ s^{-1}$) Torr is used instead of the high field mobility k used to describe ion drift motion in the sheaths.

Thus, the ambipolar diffusion Eq. (22) is solved for $d_{ps} \leqslant x \leqslant d_{gs}$, with the boundary conditions

$$D_a \left| \frac{\partial n_i}{\partial x} \right|_{X=d_{ps}} = \frac{J_{ip}}{e} \quad \text{and} \quad D_a \left| \frac{\partial n_i}{\partial x} \right|_{X=d_{gs}} = \frac{J_{ig}}{e}$$

$$n_i|_{x=d_{ps}} = N_{ps} \quad \text{and} \quad n_i|_{x=d_{gs}} = N_{gs},$$

where d_{pd}, d_{gd} are the mean powered and grounded sheath lengths, J_{ip}, J_{ig} the ion conduction current densities, and N_{pd}, N_{gd} the charge densities at bulk-powered and grounded sheath boundaries, respectively.

Furthermore, the distribution of the ambipolar electric field E_{ab} is calculated using the equation[24]

$$E_{ab} = -T_e \frac{1}{n_i} \frac{dn_i}{dx}. \tag{21}$$

The results of the earlier calculations at different excitation frequencies and conditions of constant power dissipation are summarized in Table I.

C. Power dissipation

The calculation of the ion flux density in both sheaths permits the estimation of the power consumed for ion acceleration[22]

$$P_i = V_s I_i. \tag{22}$$

The power consumed for electron heating can then be distinguished as the difference between the total power consumed in the discharge and the power consumed for ion acceleration

$$P_e = P_{TOT} - (P_{ips} + P_{igs}). \tag{23}$$

TABLE II. The power consumed for electron heating P_e, the power consumed for ion acceleration at the powered and the grounded sheath P_{ip}, P_{ig} and the mean collision frequency for momentum transfer ν_m, as calculated from the model of power dissipation in the discharge.

Frequency (MHz)	P_e (W)	P_{ip} (W)	P_{ig} (W)	υ_m (10^9 Hz)
13.56	4.38	0.17	0.032	6.32
30	4.50	0.07	0.024	3.84
35	4.53	0.06	0.018	2.97
50	4.62	0.03	0.010	1.86

In order to relate the different paths of power dissipation with the ohmic part of the discharge impedance, an in series equivalent circuit is assumed for the discharge.[17,22]

The resistance related with ion acceleration in the powered and grounded sheath is calculated using the formulas[22]

$$R_{ips} = \frac{2V_{ps}I_{ips}}{I_d^2} \quad \text{and} \quad R_{igs} = \frac{2V_{ps}I_{ips}}{(fI_d)^2}. \tag{24}$$

The resistive component R_ν related with electron-molecule collisions is then calculated using the expression

$$R_\upsilon = R - (R_{ips} + R_{igs}), \tag{25}$$

where R the total resistive component as calculated from Eq. (5), is strictly related to the frequency at which the electrons relax their momentum[22]

$$\tilde{\upsilon}_m = \frac{R_\upsilon A e^2 n_{av}}{d_b m_e}, \tag{26}$$

where n_{av} (Table I), is the average plasma density and d_b the bulk length.

The results concerning power dissipation at different frequencies are summarized in Table II.

D. Electron heating and mean electron energy

The power consumed for electron heating P_e that has been calculated earlier represents the total power transferred to electrons. However, significant variations are expected in the spatial distribution of electron heating. In order to follow the changes in the spatial variation of electron heating, the time-averaged power transferred per electron θ can be used. This parameter can be expressed as a function of the time averaged electric field and the electron-molecule collision frequency

$$\theta(x) = \frac{e^2}{m_e} \frac{\tilde{\upsilon}_m}{\tilde{\upsilon}_m^2 + \omega^2} \frac{E_b^2(x)}{2}. \tag{27}$$

The changes in electron heating will be reflected in the value of the mean electron energy, resulting from the balance between the energy gained from the field and the energy lost per collision:

$$\frac{d\bar{\varepsilon}}{dt} = e u_e E_{eff} - \overline{\kappa \tilde{\upsilon}_m \varepsilon}, \tag{28}$$

where the value of the effective (ohmic) part of the rf bulk electric field has been used

TABLE III. The power transferred per electron θ, mean collision frequency for energy transfer ν_e, electron oscillatory drift velocity u_e, and mean electron energy ε, as calculated in Sec. IV D. The drift velocities of ions u_{ip+}, u_{ig+} at the powered and grounded plasma-sheath boundaries are also included.

Frequency (MHz)	θ 10^{-13} W	u_{ip+} 10^6 (cm/s)	u_{ig+} 10^6 (cm/s)	u_e 10^7 (cm/s)	ν_e (10^7 Hz)	ε (eV)
13.56	29.8	1.43	0.91	2.72	12.6	3.3
30	6.48	1.21	0.81	2.62	7.7	2.7
35	3.71	1.12	0.81	2.38	5.9	2.4
50	2.3	0.92	0.68	2.01	3.7	1.8

$$E_{\text{eff}}=\frac{E_b}{\sqrt{2}}\frac{\tilde{\nu}_m}{\sqrt{\tilde{\nu}_m^2+\omega^2}}, \tag{29}$$

u_e is the electron drift velocity and $\bar{\kappa}$ is the mean energy loss factor. In fact, $\bar{\kappa}$ is a function of electron energy and in our case where mean electron energy is around 2 eV, the value of $\bar{\kappa}$ is assumed to be 0.05.[29]

Assuming a sinusoidal rf field and substituting electron drift velocity as[35]

$$u_e=\frac{eE_{\text{eff}}}{m_e\sqrt{\tilde{\nu}_m^2+\omega^2}}\sin(\omega t-\varphi), \tag{30}$$

where $\phi=\tan^{-1}(\omega/\nu_m)$ is the angle by which the electron drift motion lags the field Eq. (28) results in a differential equation of the form

$$\frac{d\bar{\varepsilon}}{dt}=\frac{e^2E_{\text{eff}}^2}{m_e\sqrt{\tilde{\nu}_m^2+\omega^2}}\sin\omega t\sin(\omega t-\phi)-\tilde{\nu}_e\bar{\varepsilon} \tag{31}$$

that has the solution

$$\bar{\varepsilon}=\frac{e^2E_{\text{eff}}^2}{2\tilde{\nu}_e m_e\sqrt{\tilde{\nu}_m^2+\omega^2}}\times\left[\cos(-\phi)-\frac{\cos(2\omega t-\phi)+(2\omega/\tilde{\nu}_e)\sin(2\omega t-\phi)}{1+(2\omega/\tilde{\nu}_e)^2}\right], \tag{32}$$

where ν_e is the mean collision frequency for energy transfer, resulting from the product of $\bar{\kappa}$ times ν_m. The term $eE_{\text{eff}}^2/(\tilde{\nu}_e m_e\sqrt{\tilde{\nu}_m^2+\omega^2})=\varepsilon_{\text{dc}}$ can be attributed to the mean electron energy that would be observed in a dc electric field of strength E_{eff}.

The calculated values of the mean electron energy and the power transferred per electron, at different frequencies and conditions of constant power dissipation, are summarized in Table III.

V. DISCUSSION

The increase of the excitation frequency, under constant power conditions, has a primary influence on the ion motion in the discharge leading to a continuous decrease of the ion ambipolar velocity in the bulk and the drift velocity in the sheaths. This is followed by a reduction of the charge loss rates, at both electrodes, as shown in Fig. 6, that is more significant for the powered electrode. This decrease of the charge loss rate imposes an analogous behavior for the ionization rate (Fig. 5).

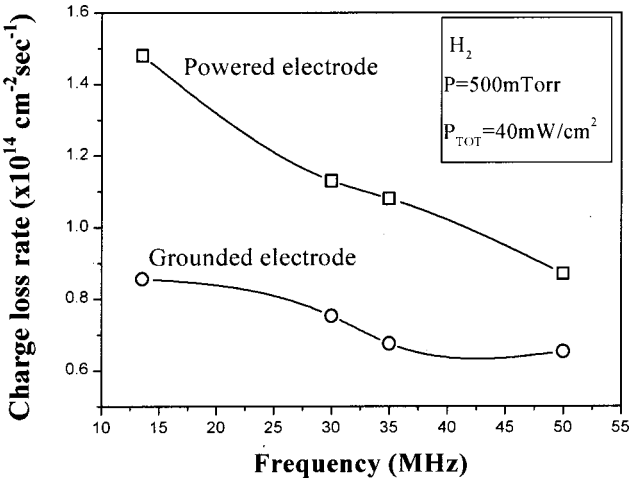

FIG. 6. Charge loss rates at both powered and grounded electrodes calculated from the ion conduction current, as a function of the driving frequency.

The decrease of the ion drift-diffusion velocity is followed by a gradual enhancement of electron trapping in the bulk, since electron motion in the glow is also mostly controlled by diffusion. This is shown in Fig. 7, presenting the spatial variation of the electron density, as calculated from the analysis of ion transport in the sheaths and in the bulk. As frequency increases, the electron density increases at every point of the interelectrode space while the maximum of the distribution is shifted towards the rf electrode. This results in a change of the discharge structure and a better plasma confinement, the discharge having less contact with the reactor walls. In addition, the sheaths become thinner, as calculated using electrical measurements (Table I) or seen in the emission profiles (Fig. 5).

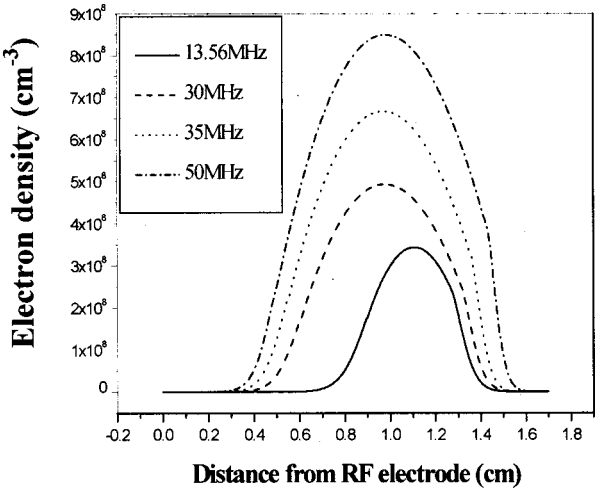

FIG. 7. Spatial distribution of electron density at four different frequencies.

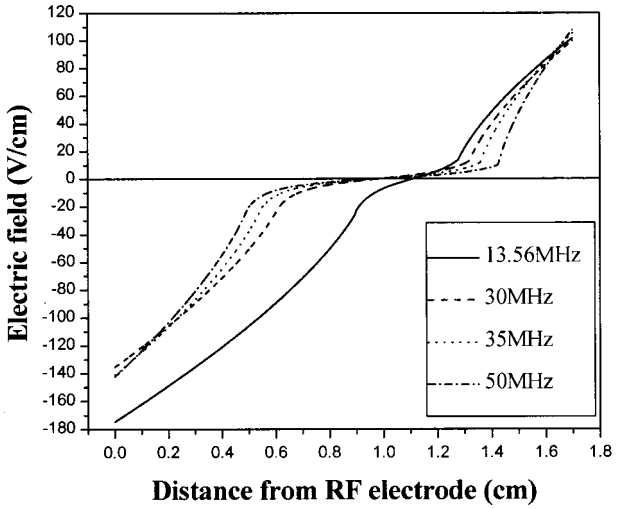

FIG. 8. Spatial variation of the time-averaged electric field.

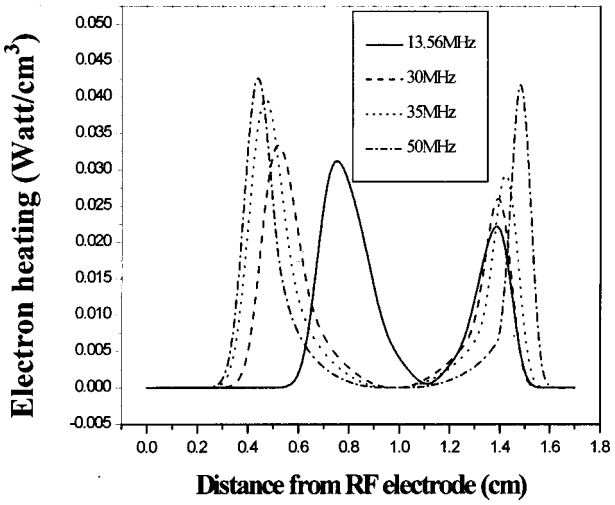

FIG. 9. Total electron heating as a function of the position in the interelectrode space at four different frequencies.

The decrease of the ion flux combined with the drop of the applied voltage with increasing frequency will also lead to a modification of the power deposition mechanisms. Thus, the fraction of power consumed for ion acceleration in both sheaths, as calculated using Eq. (22) (Table II, P_{ip}, P_{ig}) is reduced as frequency increases, due to the smaller voltage drop across the sheaths and the decrease of the ion flux. At all cases, this fraction is a small part of the total discharge power exceeding 6% only at 13.56 MHz.

Therefore, at these conditions almost all the power is used for electron acceleration (Table II, P_e). However, changes in the way electrons gain and lose energy are expected, at different frequencies. At the present experimental conditions, the discharge operates in the α regime, where interactions of the electrons with the high field oscillating sheaths and bulk ohmic heating are the primary mechanisms. In both cases, electrons gain energy from the high frequency electric field. Therefore, it is useful to review the spatial variation of the time-averaged electric field, as presented in Fig. 8. At higher frequencies, the electric field distribution in the bulk becomes more uniform, and takes lower values either in the sheaths or in the bulk. At all frequencies, the electric field is much higher in the sheaths and thus electron acceleration is expected to take place near the plasma-sheath boundary where the electric field and the electron density have sufficiently high values. Thus, as observed in Fig. 9, electron heating mostly occurs in the plasma-sheath regions, it is slightly increasing with frequency, and is always higher for the powered sheath compared to the grounded one. At 13.56 MHz due to the rather large sheath lengths, powered and grounded sheaths appear to be very close, making the distinction between sheath and bulk heating meaningless, since all electrons have the chance to interact with the sheaths at some point of the rf cycle.

On the other hand, the slight increase of total electron heating with frequency, does not lead to an enhancement of the dissociative excitation (Fig. 5) and ionization rates of hydrogen. This can be understood, if one takes into account the significantly different effect of frequency on the electron density and the total power transferred to electrons P_e. The average electron density has been found to increases significantly, scaling as $n_{\mathrm{av}} \propto \omega^{1.7}$ (Table I, Fig. 7), while the dependence of P_e on frequency appears to be almost linear, scaling as $P_e \propto \omega$ (Table II). This is consequently followed by a decrease of the power acquired per electron θ the spatial distribution of which is presented in Fig. 10. As in the case of the total electron heating, the value of θ is higher near the plasma-sheath boundaries, taking very low values in the bulk at all frequencies. Under steady-state conditions, θ reflects the balance between the rate electrons gain energy from the electric field, and the rate this energy is lost by elastic or inelastic collisions.[6] The relation of θ with electron energy losses can be expressed as

$$\theta = \left(\frac{2m}{M}\right)\langle \nu_{\mathrm{el}}(u) e u \rangle + \sum_j \nu_j^{\mathrm{in}}(u) e V_j , \tag{33}$$

where the first right-hand term represents losses in elastic collisions, while the second term losses in total inelastic collisions. In high-energy processes like excitation and ioniza-

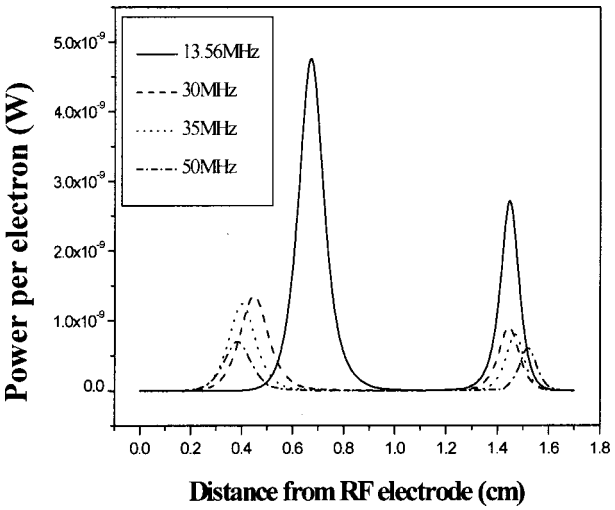

FIG. 10. Time-averaged power per electron as a function of the interelectrode space.

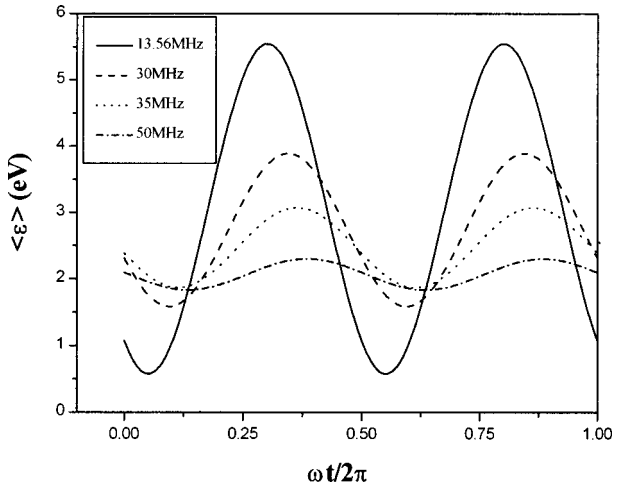

FIG. 11. Modulation of the spatially averaged mean electron energy $\langle\varepsilon\rangle$ during the rf cycle, at four different frequencies.

tion, large amounts of energy are lost per collision and thus such collisions will tend to give a rise in θ. Therefore, the observed drop of the excitation rate with increasing frequency (Fig. 5) and the analogous predicted drop of the ionization rate, are in agreement with the drop of θ. Thus, considering that the increase of the total electron power (Table II, P_e) does not lead to an enhancement of high-energy processes, the increase of frequency is expected to favor lower threshold processes (hydrogen vibrational excitation and dissociation).

The earlier interpretation of the effect of frequency on high-energy processes, based on the electron energy balance, appears to be in a good agreement with the theoretical predictions resulting from the solution of the time-dependent Boltzmann equation.[14,15] In these studies, comparison of hydrogen discharges for the same applied field, in the range of frequency ($\pi\times10^7<\omega<\pi\times10^8$) used in the present case, have shown a decrease of the mean power input per electron with increasing frequency. Power losses in excitation, dissociation and ionization of hydrogen have been found to decrease while losses to vibrational excitation and elastic collisions were increasing with frequency. In addition, the oscillation up to 40 MHz, of the electron energy distribution function (EEDF) with the high frequency field that has been reported in Refs. 14 and 15 appears also to be effective in the present case. The modulation of EEDF with the time-varied field is reflected on the temporal evolution of the mean electron energy that has been predicted using Eq. (32). The decrease of momentum υ_m (Table II) and energy υ_e (Table III) transfer collision frequencies combined to the increase of frequency, leads to a modification of the electron energy oscillation during the rf cycle that is presented in Fig. 11. As observed, the mean electron energy drops with frequency being in agreement with the earlier-mentioned decrease of the power transferred per electron θ. At 13.56 MHz, $\langle\varepsilon\rangle$ is fully modulated during the rf cycle taking values in the range from 0 to 5.5 eV, while the increase of frequency is accompanied by a continuous decrease of the mean electron energy oscillation that at 50 MHz has an almost dc behavior.

The drop of excitation and ionization rate with frequency that has been experimentally observed, can be very well explained by the electron energy balance and is in agreement with theoretical predictions. However, in all previous studies concerning the issue[7–10,13] an enhancement of dissociation and dissociative excitation rates with frequency has been observed. This discrepancy can be the result of the rather different pressure, gas, and power levels used, while the accuracy of the method used for the measurement of power can also play an important role. In the present work, the drop of the hydrogen dissociative excitation and the ionization rate is dictated by the higher increase of the electron density compared to the increase of the total power gained by electrons with frequency. Both electron density and power per electron will be affected in a different manner by changing one of the earlier mentioned discharge parameters. Further work involving different gases and pressures is in progress in order to study the effect of frequency on various energy gas-phase processes.

VI. CONCLUSIONS

Hydrogen discharges operating at different rf frequencies and in conditions of constant power dissipation have been investigated using electrical and optical diagnostics, and a theoretical discharge model.

A constant power consumption level in the discharge with increasing frequency is obtained by decreasing the operation voltage. This is followed by an increase of the discharge current and a decrease of the discharge impedance. These changes indicate variations in electron density and energy that are reflected in the outcome of electron-molecule collision processes.

The drop of the operation voltage is followed by a drop of the charge loss rates due to the lower ambipolar ion velocity in the bulk plasma and the lower ion drift velocity in the sheaths. The decrease of the ion loss rate enhances electron trapping in the bulk, resulting in a higher electron density and a lower bulk field. Therefore, the increase of the discharge current with frequency will be the result of the significant increase of electron density and a simultaneous decrease of the electron drift velocity. Furthermore, the increase of plasma density with frequency is followed by a drop of the discharge reactance due to the decrease of the sheath lengths, and a drop of discharge resistance due to the higher plasma conductivity.

The power consumed for ion acceleration has been found to decrease with frequency, being always a small fraction of the total power dissipated in the discharge, over the entire range of frequencies studied. Almost all of the power is consumed for electron acceleration, and this amount is slightly increasing with frequency. The relative increase of the electron density and the total power transferred for electron heating results in a decrease of the average power transferred per electron and consequently in a drop of the mean electron energy. Modulation of the mean electron energy during the rf cycle almost stops as frequency increases and a transition from a time dependent to a time independent

EEDF has been predicted to occur in the frequency range studied here, as the ratio of ω/υ_e crosses unity at 30 MHz.

Finally, under these conditions, hydrogen dissociative excitation and ionization rates have been found to decrease with frequency, revealing that the balance between the total electron energy gained from the field and lost in collisions with molecules is ensured at higher frequencies by an enhancement of the lower energy threshold processes.

[1] F. Finger, U. Kroll, V. Viret, and A. Shah, J. Appl. Phys. **71**, 5665 (1992).
[2] H. H. Goto, H. D. Lowe, and T. Ohmi, J. Vac. Sci. Technol. A **10**, 3048 (1992).
[3] M. Surendra and D. B. Graves, Appl. Phys. Lett. **59**, 2091 (1991).
[4] V. Vahedi, C. K. Birdsall, M. A. Lieberman, G. DiPeso, and T. D. Rognlien, Phys. Fluids B **5**, 2719 (1993).
[5] M. J. Colgan, M. Meyyappan, and D. E. Murnick, Plasma Sources Sci. Technol. **3**, 181 (1994).
[6] M. Moisan *et al.*, J. Vac. Sci. Technol. B **9**, 8 (1991).
[7] A. A. Howling, J.-L. Dorier, Ch. Hollenstein, U. Kroll, and F. Finger, J. Vac. Sci. Technol. A **10**, 1080 (1992).
[8] L. Sansonnens, A. A. Howling, and Ch. Hollenstein, Plasma Sources Sci. Technol. **7**, 114 (1998).
[9] M. Heintze, R. Zedlitz, and G. H. Bauer, J. Phys. D **26**, 1781 (1993).
[10] T. Kitajima, Y. Takeo, N. Nakano, and T. Makabe, J. Appl. Phys. **84**, 5928 (1998).
[11] V. A. Godyak and R. B. Piejak, J. Vac. Sci. Technol. A **8**, 3833 (1990).
[12] N. Spiliopoulos, D. Mataras, and D. E Rapakoulias, J. Vac. Sci. Technol. A **14**, 2757 (1996).
[13] A. C. Fozza, M. Moisan, and M. R. Wertheimer, J. Appl. Phys. **88**, 20 (2000).
[14] R. Winkler, J. Wilhelm, and A. Hess, Ann. Phys. (N.Y.) **42**, 537 (1987).
[15] R. Winkler, M. Dilorando, M. Capitelli, and J. Wilhem, Plasma Chem. Plasma Process. **7**, 125 (1987).
[16] M. A. Sobolewski, J. Vac. Sci. Technol. A **10**, 3550 (1992).
[17] C. Beneking, J. Appl. Phys. **68**, 4461 (1990).
[18] D. Mataras, S. Cavadias, and D. E. Rapakoulias, J. Appl. Phys. **66**, 119 (1989).
[19] S. Stamou, E. Amanatides, D. Mataras and D. E. Rapakoulias, in *Proceedings of 14th European Photovoltaic Solar Energy Conference*, Barcelona, 1997, p. 664.
[20] V. A Godyak, R. B. Piejak, and B. M Alexandrovich, J. Appl. Phys. **69**, 3455 (1991).
[21] M. Yan and W. J. Goedheer, Plasma Sources Sci. Technol. **8**, 349 (1999).
[22] V. A. Godyak, R. B. Piejak, and B. M. Alexandrovich, IEEE Trans. Plasma Sci. **19**, 660 (1991).
[23] S. Stamou, E. Amanatides, and D. Mataras, High Temp. Mater. Sci. **3**, 255 (1999).
[24] M. A. Lieberman, J. Appl. Phys. **65**, 4186 (1989).
[25] D. E. Gerassimou, S. Cavadias, D. Mataras, and D. E. Rapakoulias, J. Appl. Phys. **67**, 146 (1989).
[26] A. Von Engel, *Ionized Gases* (Oxford University Press, London, 1965), pp. 41 & 126.
[27] A. J. van Roosmalen and P. J. Q. van V. Vader, J. Appl. Phys. **68**, 1497 (1990).
[28] M. A. Liebermann, IEEE Trans. Plasma Sci. **17**, 338 (1989).
[29] E. W. McDaniel, *Collision Phenomena in Ionized Gases* (Wiley, New York, 1964), pp. 472 & 498.
[30] V. A. Godyak and N. Sternberg, Phys. Rev. A **42**, 2299 (1990).
[31] T. Panagopoulos and D. J. Economou, J. Appl. Phys. **85**, 3435 (1999).
[32] N. Spiliopoulos, D. Mataras, and D. Rapakoulias, Jpn. J. Appl. Phys., Part 1 **36**, 66 (1997).
[33] M. A. Sobolewski, IEEE Trans. Plasma Sci. **23**, 1006 (1995).
[34] E. Graham IV, D. R. James, W. C. Keever, D. L. Albritton, and E. W. McDaniel, J. Chem. Phys. **59**, 3477 (1973).
[35] A. M. Howatson, *An Introduction to Gas Discharges* (Pergamon, New York, 1965), p. 143.